NEW DIFFRACTION DATA

Crystal structure of nequinate, $C_{22}H_{23}NO_4$

James A. Kaduk [1,2,a], Amy M. Gindhart [3], Stacy Gates-Rector [3], and Thomas N. Blanton [3]

[1]*Illinois Institute of Technology, 3101 S. Dearborn St., Chicago, IL 60616, USA*
[2]*North Central College, 131 S. Loomis St., Naperville, IL 60540, USA*
[3]*ICDD, 12 Campus Blvd., Newtown Square, PA 19073-3273, USA*

The crystal structure of nequinate has been solved and refined using synchrotron X-ray powder diffraction data and optimized using density functional techniques. Nequinate crystallizes in the space group $P2_1/c$ (#14) with $a = 18.35662(20)$, $b = 11.68784(6)$, $c = 9.06122(4)$ Å, $\beta = 99.3314(5)°$, $V = 1918.352(13)$ Å^3, and $Z = 4$. The crystal structure is dominated by the stacking of the approximately planar molecules. N–H⋯O hydrogen bonds link adjacent molecules into chains parallel to the b-axis. The powder pattern has been submitted to ICDD for inclusion in the Powder Diffraction File™ (PDF®). © *The Author(s), 2022. Published by Cambridge University Press on behalf of International Centre for Diffraction Data. This is an Open Access article, distributed under the terms of the Creative Commons Attribution licence (http://creativecommons.org/licenses/by/4.0/), which permits unrestricted re-use, distribution and reproduction, provided the original article is properly cited.* [doi:10.1017/S0885715622000379]

I. INTRODUCTION

Nequinate is an antiprotozoan used as a coccidiostat for poultry and rabbits. Nequinate treats coccidiosis, a parasitic disease, caused by a spore-forming, single-cell protozoa called coccidia. Coccidia are from the same class of organisms (sporozoa) that cause malaria. The systematic name (CAS Registry Number 13997-19-8) is methyl 6-butyl-4-oxo-7-phenylmethoxy-1H-quinoline-3-carboxylate. A two-dimensional molecular diagram is shown in Figure 1.

We are unaware of any published X-ray diffraction data for nequinate. This work was carried out as part of a project (Kaduk *et al.*, 2014) to determine the crystal structures of large-volume commercial pharmaceuticals and include high-quality powder diffraction data for them in the Powder Diffraction File (Gates-Rector and Blanton, 2019).

II. EXPERIMENTAL

Nequinate was a commercial reagent, purchased from TargetMol (Batch #143800), and was used as-received. The white powder was packed into a 1.5 mm diameter Kapton capillary and rotated during the measurement at ~50 Hz. The powder pattern was measured at 295 K at beam line 11-BM (Antao *et al.*, 2008; Lee *et al.*, 2008; Wang *et al.*, 2008) of the Advanced Photon Source at Argonne National Laboratory using a wavelength of 0.458208(2) Å from 0.5 to 50° 2θ with a step size of 0.001° and a counting time of 0.1 s step^{-1}. The high-resolution powder diffraction data were collected using 12 silicon crystal analyzers that allow for high angular resolution, high precision, and accurate peak positions. A silicon (NIST SRM 640c) and alumina (SRM 676a) standard (ratio Al_2O_3:Si = 2:1 by weight) was used to calibrate the instrument and refine the monochromatic wavelength used in the experiment.

The pattern was indexed using JADE Pro 8.1 (MDI, 2021) and N-TREOR (Altomare *et al.*, 2013) on a high-quality primitive monoclinic unit cell with $a = 18.35662(20)$, $b = 11.68784(6)$, $c = 9.06122(4)$ Å, $\beta = 99.3314(5)°$, $V = 1918.352(13)$ Å^3, and $Z = 4$. The space group suggested by both programs was $P2_1/c$, which was confirmed by successful solution and refinement of the structure. A reduced cell search in the Cambridge Structural Database (Groom *et al.*, 2016) yielded 21 hits but no structures of nequinate derivatives.

A nequinate molecule was downloaded from PubChem (Kim *et al.*, 2019) as Conformer3D_CID_26383.sdf. It was converted into a *.mol2 file using Mercury (Macrae *et al.*, 2020) and into a Fenske-Hall Z-matrix file using OpenBabel (O'Boyle *et al.*, 2011). The structure was solved using FOX (Favre-Nicolin and Černý, 2002) using $\sin\theta/\lambda_{max} = 0.32$ Å^{-1}.
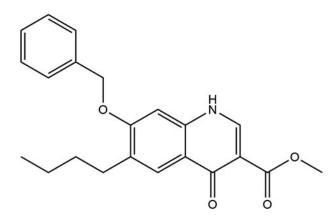

Figure 1. The 2D molecular structure of nequinate.

a)Author to whom correspondence should be addressed. Electronic mail: kaduk@polycrystallography.com

Rietveld refinement was carried out using GSAS-II (Toby and Von Dreele, 2013). Only the 1.0–25.0° portion of the pattern was included in the refinement ($d_{min} = 1.058$ Å). All non-H-bond distances and angles were subjected to restraints based on a Mercury/Mogul Geometry Check (Bruno *et al.*, 2004; Sykes *et al.*, 2011). The Mogul average and standard deviation for each quantity were used as the restraint parameters. The restraints contributed 2.3% to the final χ^2. The hydrogen atoms were included in calculated positions, which were recalculated during the refinement using Materials Studio (Dassault Systèmes, 2021). The U_{iso} were grouped by chemical similarity. The U_{iso} for the H atoms were fixed at 1.3× the U_{iso} of the heavy atoms to which they are attached. The peak profiles were described using the generalized microstrain model. The background was modeled using a 6-term shifted Chebyshev polynomial, plus a peak at 5.94° 2θ to model the scattering from the Kapton capillary and any amorphous component.

The final refinement of 109 variables using 24 039 observations and 68 restraints yielded the residuals $Rwp = 0.07133$ and goodness of fit (GOF) = 1.44. The largest peak (1.85 Å from C10) and hole (1.99 Å from O2) in the difference Fourier map were 0.18(5) and $-0.21(5)$ $e\text{Å}^{-3}$, respectively. The largest error in the difference plot (Figure 2) is in the shape of the strong low-angle (100) peak.

The structure of nequinate was optimized using Vienna Ab initio Simulation Package (VASP) (Kresse and Furthmüller, 1996) (fixed experimental unit cell) through the MedeA graphical interface (Materials Design, 2016). The calculation was carried out on 16 2.4 GHz processors (each with 4 Gb RAM) of a 64-processor HP Proliant DL580 Generation 7 Linux cluster at North Central College. The calculation used the GGA-PBE functional, a plane wave cutoff energy of 400.0 eV, and a k-point spacing of 0.5 Å^{-1} leading to a $1 \times 2 \times 2$ mesh and took ~28 h. A single-point density functional calculation (fixed experimental cell) and population analysis were carried out using CRYSTAL17 (Dovesi *et al.*, 2018). The basis sets for the H, C, N, and O atoms in the calculation were those of Gatti *et al.* (1994). The calculations were run on a 3.5 GHz PC using 8 k-points and the B3LYP functional, and took ~2.6 h.

III. RESULTS AND DISCUSSION

The root-mean-square (rms) Cartesian displacement between the Rietveld-refined and density functional theory (DFT)-optimized structures of nequinate is 0.106 Å (Figure 3); the maximum deviation is 0.299 Å at the methyl group C17. The excellent agreement provides strong evidence that the structure is correct (van de Streek and Neumann, 2014). This discussion concentrates on the DFT-optimized structure. The asymmetric unit (with atom numbering) is illustrated in Figure 4. The crystal structure is shown in Figure 5 and is dominated by the stacking of the approximately planar molecules. The mean plane is approximately (8,−1,9). The molecules form layers parallel to the *bc*-plane. The interlayer contacts are hydrocarbon–hydrocarbon. All of the bond distances, bond angles, and torsion angles fall within the normal ranges indicated by a Mercury Mogul Geometry check (Macrae *et al.*, 2020).

Quantum chemical geometry optimization of the nequinate molecule (DFT/B3LYP/6-31G*/water) using Spartan '18 (Wavefunction, Inc., 2020) indicated that the observed conformation is 2.7 kcal mol^{-1} higher in energy than the local minimum, which is, in general, similar, but has a different orientation of the C35–40 phenyl ring. A conformational analysis (MMFF force field) shows that the observed solid-state conformation is 2.3 kcal mol^{-1} higher in energy than the global minimum-energy conformation of an isolated molecule. The main difference is in the orientation of the methyl ether. The differences show that, despite the weak intermolecular interactions, they are important in determining the solid-state conformation.

Analysis of the contributions to the total crystal energy of the structure using the Forcite module of Materials Studio (Dassault Systèmes, 2021) suggests that bond, angle, and torsion distortion terms contribute significantly to the intra-
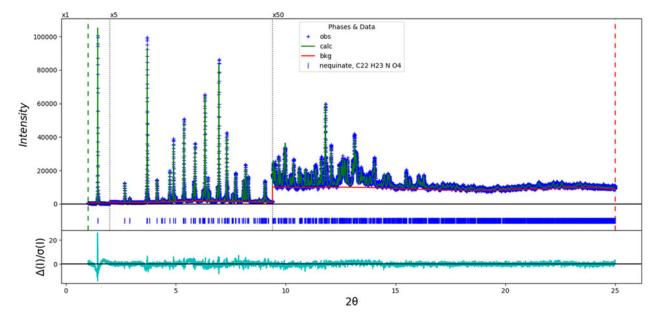

Figure 2. The Rietveld plot for the refinement of nequinate. The blue crosses represent the observed data points, and the green line is the calculated pattern. The cyan curve is the normalized error plot. The vertical scale has been multiplied by a factor of 5× for $2\theta > 2.0°$ and by a factor of 50× for $2\theta > 9.4°$.
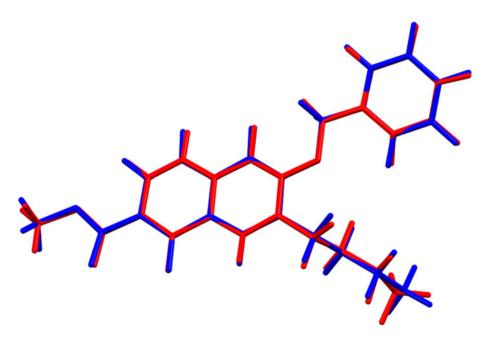
Figure 3.   Comparison of the Rietveld-refined (red) and VASP-optimized (blue) structures of nequinate. The rms Cartesian displacement is 0.106 Å.
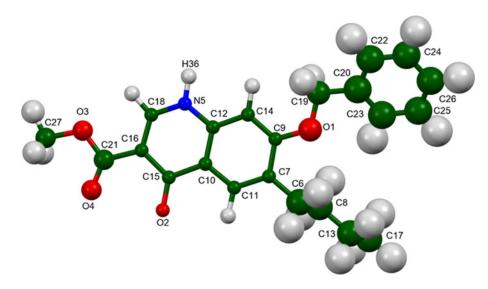

Figure 4.   The asymmetric unit of nequinate, with the atom numbering. The atoms are represented by 50% probability spheroids.

molecular deformation energy. The intermolecular energy is dominated by van der Waal's attractions and electrostatic repulsions, which, in this force field analysis, also include hydrogen bonds. The hydrogen bonds are better analyzed using the results of the DFT calculation.

There is only one traditional hydrogen bond in the structure (Table I) between the amino group N5–H36 and the carbonyl group O2. The energy of this hydrogen bond was calculated using the correlation of Wheatley and Kaduk (2019). These hydrogen bonds link adjacent molecules into chains parallel to the *b*-axis. Several inter- and intra-molecular C–H⋯O hydrogen bonds also contribute to the lattice energy.

The volume enclosed by the Hirshfeld surface of the nequinate molecule (Figure 6, Hirshfeld, 1977; Turner *et al.*, 2017) is 471.40 Å^3, 98.29% of 1/4 the unit cell volume. The packing density is thus fairly typical. The only significant close contacts (red in Figure 6) involve the hydrogen bonds.

The volume/non-hydrogen atom is typical for pharmaceuticals, at 17.8 Å^3.

The Bravais–Friedel–Donnay-Harker (Bravais, 1866; Friedel, 1907; Donnay and Harker, 1937) algorithm suggests that we might expect platy morphology for nequinate, with {100} as the major faces. A second-order spherical harmonic model was included in the refinement. The texture index was 1.029(0), indicating that preferred orientation was slight in this rotated capillary specimen. The powder pattern of nequinate from this synchrotron data set has been submitted to ICDD for inclusion in the Powder Diffraction File.

IV. DEPOSITED DATA

The Crystallographic Information Framework (CIF) files containing the results of the Rietveld refinement (including the
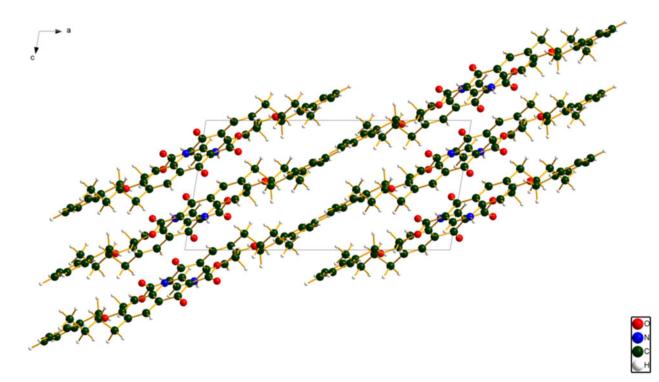
Figure 5. The crystal structure of nequinate, viewed down the *b*-axis.

TABLE I. Hydrogen bonds (CRYSTAL17) in nequinate.

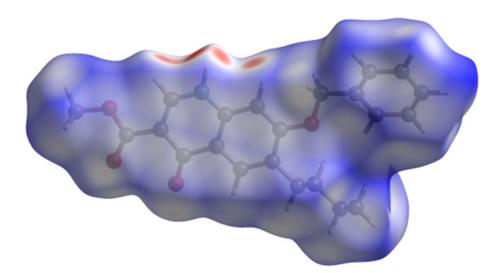| H-Bond	D–H (Å)	H⋯A (Å)	D⋯A (Å)	D–H⋯A (°)	Overlap (e)	K (kcal mol^{-1})
N5–H36⋯O2	1.038	1.970	2.756	130.1	0.043	4.8
C14–H35⋯O4	1.089	2.242	3.192	144.5	0.026	
C18–H40⋯O2	1.088	2.274	2.918	115.9	0.018	
C18–H40⋯O3	1.088	2.326[a]	2.661	95.6	0.012	
C11–H32⋯O2	1.092	2.473[a]	2.823	97.0	0.013	
C19–H41⋯O4	1.103	2.528	3.470	142.7	0.012	

[a]Intramolecular.

Figure 6. The Hirshfeld surface of nequinate. Intermolecular contacts longer than the sums of the van der Waal's radii are colored blue, and contacts shorter than the sums of the radii are colored red. Contacts equal to the sums of radii are white.

raw data) and the DFT geometry optimization were deposited with the ICDD. The data can be requested at info@icdd.com.

ACKNOWLEDGEMENTS

CONFLICTS OF INTEREST

The authors have no conflicts of interest to declare.

Altomare, A., Cuocci, C., Giacovazzo, C., Moliterni, A., Rizzi, R., Corriero, N., and Falcicchio, A. (**2013**). "EXPO2013: a kit of tools for phasing crystal structures from powder data," J. Appl. Crystallogr. **46**, 1231–1235.

Antao, S. M., Hassan, I., Wang, J., Lee, P. L., and Toby, B. H. (**2008**). "State-of-the-art high-resolution powder X-ray diffraction (HRPXRD) illustrated with Rietveld refinement of quartz, sodalite, tremolite, and meionite," Can. Mineral. **46**, 1501–1509.

Bravais, A. (**1866**). *Etudes Cristallographiques* (Gauthier Villars, Paris).

Bruno, I. J., Cole, J. C., Kessler, M., Luo, J., Motherwell, W. D. S., Purkis, L. H., Smith, B. R., Taylor, R., Cooper, R. I., Harris, S. E., and Orpen, A. G. (**2004**). "Retrieval of crystallographically-derived molecular geometry information," J. Chem. Inf. Sci. **44**, 2133–2144.

Dassault Systèmes (**2021**). *Materials Studio 2021* (BIOVIA, San Diego, CA).

Donnay, J. D. H. and Harker, D. (**1937**). "A new law of crystal morphology extending the law of Bravais," Am. Mineral. **22**, 446–447.

Dovesi, R., Erba, A., Orlando, R., Zicovich-Wilson, C. M., Civalleri, B., Maschio, L., Rerat, M., Casassa, S., Baima, J., Salustro, S., and Kirtman, B. (**2018**). "Quantum-mechanical condensed matter simulations with CRYSTAL," WIREs Comput. Mol. Sci. **8**, e1360.

Favre-Nicolin, V. and Černý, R. (**2002**). "FOX, free objects for crystallography: a modular approach to ab initio structure determination from powder diffraction," J. Appl. Crystallogr. **35**, 734–743.

Friedel, G. (**1907**). "Etudes sur la loi de Bravais," Bull. Soc. Fr. Mineral. **30**, 326–455.

Gates-Rector, S. and Blanton, T. (**2019**). "The powder diffraction file: a quality materials characterization database," Powd. Diffr. **39**(4), 352–360.

Gatti, C., Saunders, V. R., and Roetti, C. (**1994**). "Crystal-field effects on the topological properties of the electron-density in molecular crystals – the case of urea," J. Chem. Phys. **101**, 10686–10696.

Groom, C. R., Bruno, I. J., Lightfoot, M. P., and Ward, S. C. (**2016**). "The Cambridge structural database," Acta Crystallogr. Sect. B: Struct. Sci., Cryst. Eng. Mater. **72**, 171–179.

Hirshfeld, F. L. (**1977**). "Bonded-atom fragments for describing molecular charge densities," Theor. Chem. Acta **44**, 129–138.

Kaduk, J. A., Crowder, C. E., Zhong, K., Fawcett, T. G., and Suchomel, M. R. (**2014**). "Crystal structure of atomoxetine hydrochloride (Strattera), $C_{17}H_{22}NOCl$," Powd. Diffr. **29**(3), 269–273.

Kim, S., Chen, J., Cheng, T., Gindulyte, A., He, J., He, S., Li, Q., Shoemaker, B. A., Thiessen, P. A., Yu, B., Zaslavsky, L., Zhang, J., and Bolton, E. E. (**2019**). "Pubchem 2019 update: improved access to chemical data," Nucleic Acids Res. **47**(D1), D1102–D1109. doi:10.1093/nar/gky1033.

Kresse, G. and Furthmüller, J (**1996**). "Efficiency of Ab-initio total energy calculations for metals and semiconductors using a plane-wave basis set," Comput. Mater. Sci. **6**, 15–50.

Lee, P. L., Shu, D., Ramanathan, M., Preissner, C., Wang, J., Beno, M. A., Von Dreele, R. B., Ribaud, L., Kurtz, C., Antao, S. M., Jiao, X., and Toby, B. H. (**2008**). "A twelve-analyzer detector system for high-resolution powder diffraction," J. Synch. Rad. **15**(5), 427–432.

Macrae, C. F., Sovago, I., Cottrell, S. J., Galek, P. T. A., McCabe, P., Pidcock, E., Platings, M., Shields, G. P., Stevens, J. S., Towler, M., and Wood, P. A. (**2020**). "*Mercury 4.0*: from visualization to design and prediction," J. Appl. Crystallogr. **53**, 226–235.

Materials Design (**2016**). *MedeA 2.20.4* (Materials Design Inc., Angel Fire, NM).

MDI (**2021**). *JADE Pro Version 8.1 (Computer Software)* (Materials Data, Livermore, CA, USA).

O'Boyle, N., Banck, M., James, C. A., Morley, C., Vandermeersch, T., and Hutchison, G. R. (**2011**). "Open babel: an open chemical toolbox," J. Chem. Informatics **3**, 33. doi:10.1186/1758-2946-3-33.

Sykes, R. A., McCabe, P., Allen, F. H., Battle, G. M., Bruno, I. J., and Wood, P. A. (**2011**). "New software for statistical analysis of Cambridge structural database data," J. Appl. Crystallogr. **44**, 882–886.

Toby, B. H. and Von Dreele, R. B. (**2013**). "GSAS II: the genesis of a modern open source all purpose crystallography software package," J. Appl. Crystallogr. **46**, 544–549.

Turner, M. J., McKinnon, J. J., Wolff, S. K., Grimwood, D. J., Spackman, P. R., Jayatilaka, D., and Spackman, M. A. (**2017**). *CrystalExplorer17.* (University of Western Australia). Available at: http://hirshfeldsurface.net.

van de Streek, J. and Neumann, M. A. (**2014**). "Validation of molecular crystal structures from powder diffraction data with dispersion-corrected density functional theory (DFT-D)," Acta Cryst. Sect. B: Struct. Sci., Cryst. Eng. Mater. **70**(6), 1020–1032.

Wang, J., Toby, B. H., Lee, P. L., Ribaud, L., Antao, S. M., Kurtz, C., Ramanathan, M., Von Dreele, R. B., and Beno, M. A. (**2008**). "A dedicated powder diffraction beamline at the advanced photon source: commissioning and early operational results," Rev. Sci. Inst. **79**, 085105.

Wavefunction, Inc. (**2020**). Spartan '18 Version 1.4.5 (Wavefunction Inc., Irvine, CA).

Wheatley, A. M. and Kaduk, J. A. (**2019**). "Crystal structures of ammonium citrates," Powd. Diffr. **34**, 35–43.